DRAFT - Low turbulence levels in Wendelstein 7-X thanks to the stabilising property of kinetic electrons

J. H. E. Proll,[1] P. Xanthopoulos,[2] P. Helander,[2] G. G. Plunk,[2] B. J. Faber,[3,4] and T. Görler[5]

[1]*Science and Technology of Nuclear Fusion, Department of Applied Physics, Eindhoven University of Technology, 5600 MB Eindhoven, The Netherlands*

[2]*Max-Planck-Institut für Plasmaphysik, Wendelsteinstraße 1, 17491 Greifswald, Germany*

[3]*HSX Plasma Lab, University of Wisconsin-Madison, Madison, Wisconsin 53706, USA*

[4]*Department of Physics, University of Wisconsin-Madison, Madison, Wisconsin 53706, USA*

[5]*Max-Planck-Institut für Plasmaphysik, Boltzmanstraße 2, 85748 Garching, Germany*

(Dated: May 19, 2017)

Abstract

How the magnetic geometry of a magnetic confinement fusion device affects the levels of turbulent transport has long been an open question and first results have only recently started to emerge. Here extensive simulation results of collisionless, electrostatic trapped-electron-mode (TEM) and ion-temperature-gradient mode (ITG) turbulence obtained with the GENE code in different magnetic geometries are presented. Among the three devices under investigation, the nearly quasi-isodynamic stellarator Wendelstein 7-X has the lowest TEM heat flux compared with the quasi-symmetric stellarator HSX and the tokamak DIII-D. The enhanced stability is in line with previous analytical predictions and also with previous linear simulation results, where it was shown that, in exactly and nearly quasi-isodynamic configurations with the maximum-J property, the classical electron-driven TEM is stable in a large part of parameter space. Additional investigations into the saturation mechanism for TEM turbulence in Wendelstein 7-X reveal that zonal flows, which are thought to be the main saturation mechanism in tokamak geometry, are much weaker in the Wendelstein 7-X geometry and it must thus be other mechanisms that provide the saturation.

INTRODUCTION

In magnetic confinement fusion devices, there are usually three processes limiting the energy confinement: radiation losses, collisional diffusion, including the effect of particle drifts that arise due to gradients and curvature of the confining magnetic field, and turbulence. While tokamaks were never critically affected by the collisional transport thanks to their axisymmetry, stellarators historically suffered from bad confinement due to the lack of symmetry and the resulting high neoclassical transport losses. Optimised stellarators using the concepts of quasi-symmetry [1, 2] - like the quasi-helically symmetric experiment HSX [3] in Madison, Wisconsin, USA - or quasi-isodynamicity [4, 5] - like the newly operational superconducting stellarator Wendelstein 7-X [6, 7] in Greifswald, Germany - are designed to overcome the problem of the neoclassical transport [8, 9]. In tokamaks the remaining problem of turbulence has already been studied extensively, and some of the most impressive theoretical results include fully-radial turbulence simulations [10], the matching of calculated fluxes with experimental results [11], multi-scale simulations including both the ion- and the electron scale [12], and faster-than-real-time modelling of turbulence using neural networks [13]. In stellarators with their more complex three-dimensional geometry, the most recent advances do not go quite as far.

As in tokamaks, ion-temperature-gradient modes (ITGs) and trapped-electron modes (TEM) have been identified as the most transport-relevant amongst the electrostatic modes. ITG-ae - ITGs with adiabatic electrons (which is usually considered a fair approximation) - have been studied thoroughly both analytically [14] and numerically in different geometries [15–17] and most recently some new findings about their saturation mechanism have been published [18, 19]. Furthermore, simulations covering an entire flux-surface have revealed an enhanced stability for strongly shaped plasmas like that of W7-X [20], and optimisation strategies towards stellarators with reduced ITG-turbulence have been demonstrated [21–24].

Due to the enhanced complexity of the system, analytical calculations as well as numerical simulations including kinetic electrons, are less numerous. In [25, 26] it was shown analytically that quasi-isodynamic stellarators with the maximum-J property (where J is the second adiabatic invariant, which is constant on flux surfaces and has a maximum on the magnetic axis) are stable towards collisionless electron-driven trapped-electron modes for $0 < \eta_e = L_n/L_{T_e} < 2/3$. Here L_{T_e} or L_n are the electron-temperature gradient scale length or density gradient scale length respectively. Later it was shown [27] that this enhanced stability also holds for W7-X, which is

	ITG-ae	ITG-ke	TEM a/L_n	TEM a/L_{T_e}
DIII-D	192,64,64,48,20,0.05	192,64,64,48,20,0.05	192,48,64,48,20,0.05	192,48,64,32,10,0.05
HSX	128,32,64,36,16,0.05	384,72,64,36,8,0.05	192,48,64,36,16,0.01	192,48,128,48,10,0.1
W7-X	384,64,128,48,20,0.05	256,64,96,48,10,0.05	256,64,96,48,10,0.05	256,256,96,48,10,0.05

TABLE I: Resolution for turbulence simulations (nkx, nky, nz, nv, nw, kymin)

only approximately quasi-isodynamic. All these results were, however, only linear results and the question arose whether the enhanced stability also holds nonlinearly. (Very recently, a nonlinear stability result has been obtained analytically [**?**]). First simulations have confirmed that this is indeed the case [29] and the present paper presents more extensive and thorough investigations into how the geometry affects TEM turbulence and ITG-ke turbulence (i.e. ITGs with kinetic electrons) by comparing extensive simulation results obtained in W7-X, HSX and the shaped tokamak DIII-D [30].

GYROKINETIC MODEL

The collisionless electrostatic simulations were performed with the Eulerian code GENE [31], which solves the gyrokinetic equation together with Maxwell's equations and is able to treat realistic geometry when coupled to the GIST code [32]. For W7-X and HSX the flux tubes studied were the so-called bean-flux tubes (i.e. where the outboard midplane of the bean cross section is passed at the centre of the flux tube), and in all three devices the flux surface chosen was at half normalised flux, i.e. $s = \psi/\psi_0 = 0.5$. For more information about the geometries studied the reader is referred to [27] for DIII-D and W7-X and to [33] for HSX. After extensive convergence tests, the resolution was chosen as seen in Table I. For the TEMs in HSX $k_y\rho_s = 0.1$ was found to be sufficient as a smallest wave number. More details can be found in [34]. For the electron-temperature-gradient-driven TEM with $a/L_{T_e} = 3$ and $a/L_n = 0$ the temperature ratio was chosen as $T_e/T_i = 7$. This way small-scale ETGs were suppressed while (at least linearly) the TEMs were not affected and the simulations were doable - otherwise the number of modes needed would have been too large in order to also consider the smaller but still contributing scales.

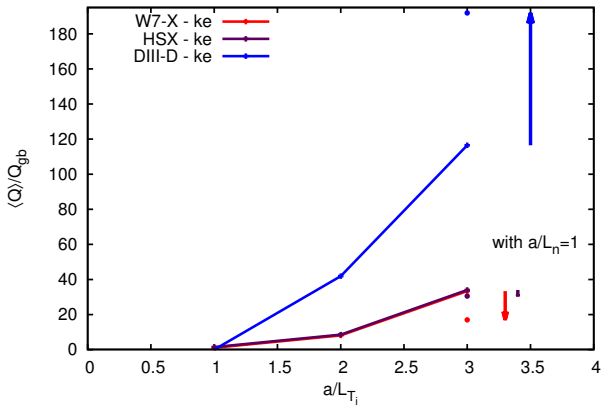

FIG. 1: Heat fluxes Q (given in gyro-bohm units) in W7-X, HSX and DIII-D for ion-temperature-gradient-driven turbulence with kinetic electrons. The full circles show how the heat fluxes change for an ion-temperature gradient of $a/L_{T_i} = 3$ once a small density gradient $a/L_n = 1$ is present.

NONLINEAR SIMULATION RESULTS

Ion-temperature-gradient modes (ITG)

First, we study the effect of the geometry on ITGs by setting the electron-temperature gradient and the density gradient to zero and by varying the ion temperature gradient a/L_{T_i}. It is observed that the heat flux (normalised to the gyro-Bohm value) of ITG-ke is smaller in both stellarators than in DIII-D, see Fig. 1. For W7-X, this had already been observed linearly [27]. As soon as there is a small density gradient of $a/L_n = 1$ present, the heat flux in W7-X is reduced significantly. Even though a reduction is also observed for HSX, it is less strong, while a strong increase in the heat flux is observed in DIII-D. Although kinetic electrons are generally destabilising in all three cases, they are less so in W7-X once a density gradient is present due to the fact that the electrons are linearly stabilising in that case [25, 26]. If we compare Figs. 1 and 2 we note that the heat fluxes of ITG-ke are much larger than those of the ITG-ae. This is rather surprising since linearly the ITG-ke (see Fig. 4) are only slightly more unstable than ITG-ae (see Fig. 3) and it is not clear where this large difference in the heat flux comes from. Since it is usually the ITG-ae case that is studied extensively, one should always keep this expected increase of the heat flux in mind. General dependencies and trends regarding the influence of the magnetic geometry on the heat fluxes are however very similar for ITG-ae and ITG-ke. For all three devices, the particle fluxes are observed to be very small and changes little for the two stellarators even if a density

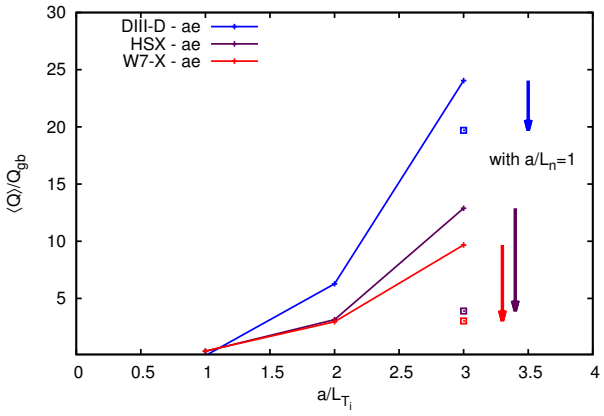

FIG. 2: Heat fluxes Q (given in gyro-bohm units) in W7-X, HSX and DIII-D for ion-temperature-gradient-driven turbulence with adiabatic electrons. The squares show how the heat fluxes change for an ion-temperature gradient of $a/L_{T_i} = 3$ once a small density gradient $a/L_n = 1$ is present.

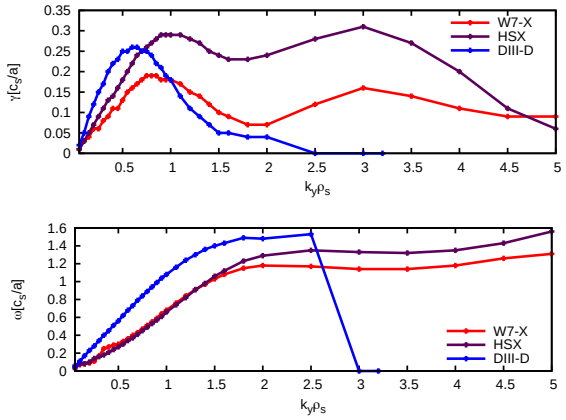

FIG. 3: Growth rates γ and real frequencies ω of ITGs with adiabatic electrons (ITG-ae) in W7-X, HSX and DIII-D.

gradient is present (Fig. 5). In DIII-D a strong increase in the particle flux is observed when $a/L_{T_i} = 3, a/L_n = 1$.

Trapped-electron modes (TEM)

For the TEM studies both temperature gradients are set to zero and only the density gradient is varied. It is found that the analytically and linearly numerically predicted enhanced stability of

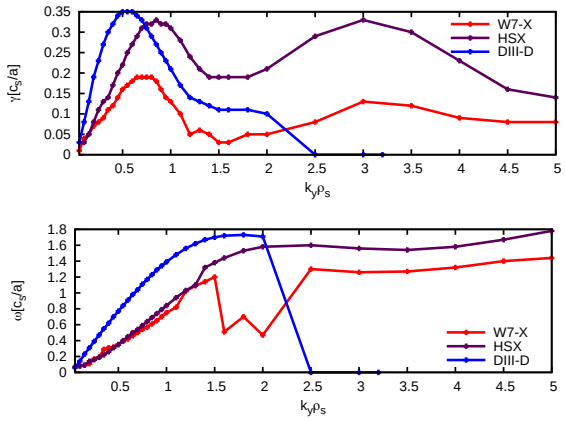

FIG. 4: Growth rates γ and real frequencies ω of ITGs with kinetic electrons (ITG-ke) in W7-X, HSX and DIII-D.

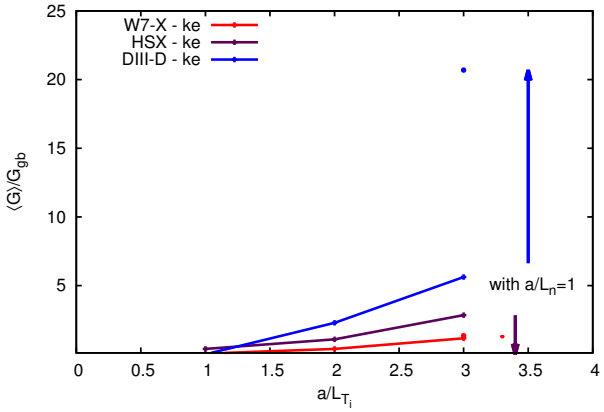

FIG. 5: Particle fluxes G (given in gyro-bohm units) in W7-X, HSX and DIII-D for ion-temperature-gradient-driven turbulence with kinetic electrons. The full circles show how the particle fluxes change for an ion-temperature gradient of $a/L_{T_i} = 3$ once a small density gradient $a/L_n = 1$ is present.

W7-X towards TEMs also prevails nonlinearly and that the heat flux is lower by up to two orders of magnitude compared with DIII-D, see Fig. 6. Even though the heat flux is small compared with DIII-D, it is still large compared with the neoclassical flux at typical parameters of density $n = 1 - 1.510?20/m?3$ and temperature $T = 1 - 3keV$ which is only around $Q \approx 0.1 Q_{GB}$ and lower [35], establishing turbulent transport as the dominant transport channel in W7-X. Compared with HSX the (turbulent) heat flux in W7-X is not much lower. This can partly be explained by the difference in linear growth rates (see Fig. 7) - HSX has maximum growth rates comparable to those of DIII-D, however, the peak occurs at much higher wave number k_y, and the more

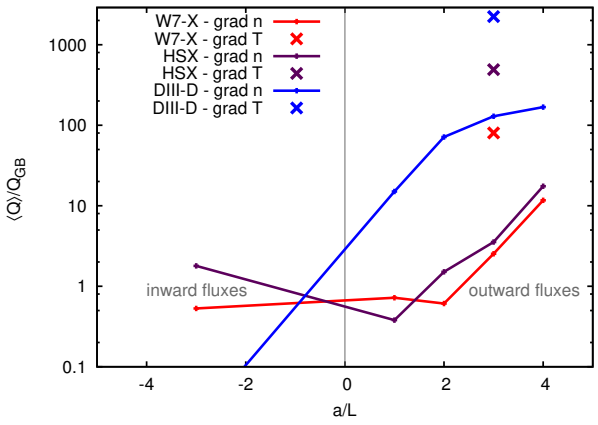

FIG. 6: Heat fluxes Q (given in gyro-bohm units) in W7-X, HSX and DIII-D for density-gradient-driven turbulence with kinetic electrons. The crosses show the heat fluxes for an electron-temperature gradient of $a/L_{T_e} = 3$ without a density gradient present.

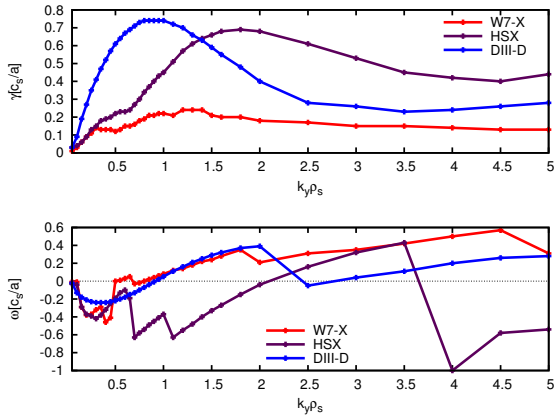

FIG. 7: Growth rates γ and real frequencies ω for density-gradient-driven modes in W7-X, HSX and DIII-D over the transport-relevant range of wave numbers k_y. The density gradient here is $a/L_n = 3$.

transport-relevant large scales at small k_y are more stable than for DIII-D. W7-X has growth rates only about a factor three lower than DIII-D. This disproportionately strong nonlinear stabilisation in W7-X becomes especially apparent when comparing the multiplying factors used in the quasi-linear estimates $Q_{QL} \propto \gamma / < k_\perp^2 >$ (Fig. 10) - the factor used for DIII-D is 44.11, while it is only 0.923 for W7-X. It is not yet clear where the strong difference comes from. There seems to be a transition to another kind of mode - the ion-driven trapped electron mode (ITEM) described recently by Plunk *et al.* in [36] - which might have different nonlinear properties. If we assume that the enhanced stability of W7-X in indeed thanks to its high degree of quasi-isodynamicity

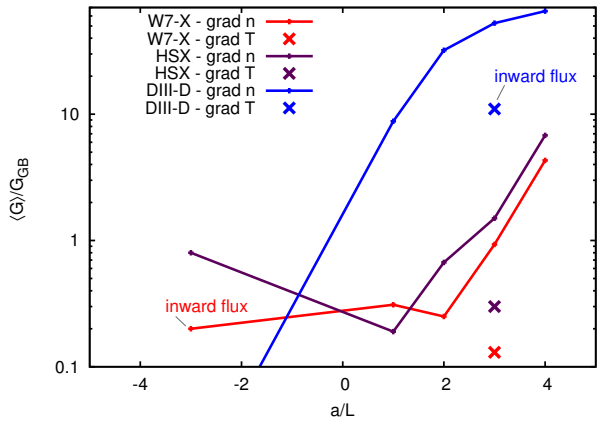

FIG. 8: Particle fluxes G (given in gyro-bohm units) in W7-X, HSX and DIII-D for density-gradient-driven turbulence with kinetic electrons. The crosses show the particle fluxes for an electron-temperature gradient of $a/L_{T_e} = 3$ without a density gradient present.

and the lack of resonance between trapped particles and the propagation of the drift waves, one could expect an increased TEM activity when the drift wave propagation is reversed, i.e. for negative density gradients. This is however not observed (even though W7-X is not completely stable as DIII-D is in that case). Also for electron-temperature-gradient-driven TEM turbulence (! with $T_e/T_i = 7$ to ensure the suppression of ETG modes) W7-X has significantly lower heat flux than both DIII-D and HSX. This suggests that the stabilisation seems to hold even outside the analytically guaranteed stable region in parameter space with $0 < \eta < 2/3$. This extension of the stable region to all $\eta > 0$ was in fact recently shown in [36] for $\omega_d \ll \omega_*$, where ω_d is the magnetic drift frequency and ω_* the drift-wave frequency. The large disparity between DIII-D and the two stellarators is also seen in the particle flux, Fig. 8. In contrast to the heat fluxes, the particle fluxes for purely electron-temperature-gradient-driven turbulence are lower than those for the density-gradient-driven turbulence. One observation that is very surprising is that $Q(a/L_n = 1) > Q(a/L_n = 2)$ (Fig. 6). The fact that the heat flux at $a/L_n = 1$ is slightly larger than that at $a/L_n = 2$ cannot be explained by the difference in linear growth rates, as can be seen in Fig. 9. The linear growth rates increase monotonically with increasing density gradient, as expected. Also the most unstable mode remains at a the same length scale, and the resulting quasi-linear estimate for the heat flux using $Q_{QL} \propto \gamma / < k_\perp^2 >$ (shown in Fig. 10 the dotted line) therefore also increases monotonically with the gradients. This could point towards a change in the saturation mechanism - either in its type or in its strength. Another possibility is that the

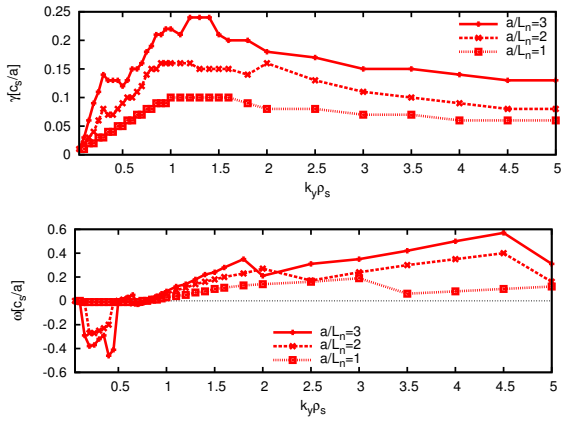

FIG. 9: Growth rates γ and real frequencies ω for density-gradient-driven modes in W7-X over the transport-relevant range of wave numbers k_y. The density gradient a/L_n is varied.

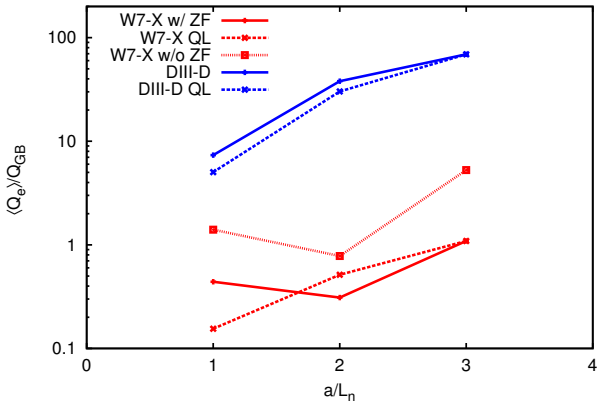

FIG. 10: Electron heat fluxes Q_e (given in gyro-Bohm units) and quasi-linear estimates for the electron heat flux for density-gradient-driven turbulence in W7-X and DIII-D. The multiplying factor to obtain the quasi-linear estimate is chosen such that the estimate matches the true nonlinear result at the highest gradient and is 44.11 for DIII-D and 0.923 for W7-X. In addition, the heat fluxes in W7-X *without* zonal flows are given ("w/o ZF" in contrast to the normal simulations "w/ ZF").

change in flux is due to phasings that are neglected in the currently-used quasi-linear estimate. For tokamaks it seems safe to assume that nothing much changes in the saturation mechanism since the quasi-linear estimate in Fig. 10 matches the true nonlinear results very well - in spite of keeping the factor multiplying $\gamma/ < k_\perp^2 >$ constant, which implicitly contains the information about saturation.

One method of studying the potential effect of zonal flows as a saturation mechanism is the

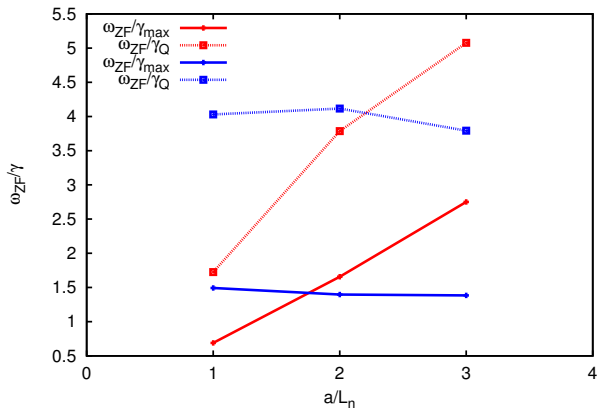

FIG. 11: The normalised zonal-flow shearing rate (normalised to either the highest growth rate γ_{max} in the wave-number scan or to the growth rate of the nonlinearly most dominant mode) for density-gradient-driven turbulence in W7-X (red) and DIII-D (blue) for a range of density gradients.

built-in capability of GENE to run a simulation without these flows - after each time step the zonal component is zeroed out. The heat fluxes are found to be about 10 times higher for all three gradients in W7-X (see Fig. 10. Also for ITGs this increase of the heat flux in W7-X by a factor of 10 has been observed [16]. However, the feature that $Q(a/L_n = 1) > Q(a/L_n = 2)$ remains, which might mean that zonal flows are not the saturation mechanism responsible for this difference in W7-X. Also, the absolute increase in heat flux when the zonal flows are zeroed out is much higher in DIII-D (not shown here) than in W7X and HSX (also not shown here, in all three cases it is a factor of about 10, which of course results in a much larger absolute increase for DIII-D) , which again supports the hypothesis that zonal flows might play a less important role in W7-X and possibly also in HSX. A similar result for ITGs were recently published in [19].

Another measure of the zonal flow strength is the normalised shearing rate ω_{ZF}/γ, where γ is chosen to be either the maximum growth rate in a scan over wave numbers *or* the growth rate of the nonlinearly dominant mode. For both choices, the difference between the devices is quite striking (Fig. 11): for DIII-D the normalised shearing rate and therefore also the zonal flow strength remain approximately constant for the different gradients. This is very much in line with the observations that the pre-factor in the quasi-linear estimate does not seem to change. In W7-X on the other hand, we observe a strong increase of the shearing rate, and thus the zonal-flow strength, with increasing gradients. This matches at least partly the observation that the absolute increase of heat flux when the zonal flows are zeroed out is highest for the density gradient

$a/L_n = 3$, which is exactly where the shearing rate is also highest.
This still does not explain why the heat flux reaches a minimum at $a/L_n = 2$, since the shearing rate there is higher than at $a/L_n = 1$. One possible explanation might come from looking at the real frequencies in Fig. 9: For both $a/L_n = 2$ and $a/L_n = 3$, modes propagating in the electron diamagnetic direction are observed at low wave numbers. At $a/L_n = 1$, however, these modes are completely absent and only modes with an almost vanishing frequency are observed. These modes might have different phasings, which would result in a wrong quasi-linear estimate, or other fundamentally different nonlinear properties and might therefore lead to an unexpected nonlinear heat flux. This could also explain why in Fig. 6 the heat fluxes of W7-X are not much lower than those in HSX.

In summary we find that the enhanced stability of W7-X prevails also nonlinearly, for both TEMs as well as ITGs when there is a density gradient present, especially when compared with DIII-D, where a disproportionately large stabilisation is observed. It seems, however, that the behaviour of the zonal flows does not sufficiently explain the trends observed in the heat fluxes.

The authors would like to thank the entire GENE team - most notably D. Told, F. Jenko, H. Doerk, A. Banon-Navarro and M.J. Pueschel - for their relentless efforts and incredible support. We would also like to thank G. Hammett, S. Lazerson, H. Mynick and J. Citrin for lots of stimulating and helpful discussions. The simulations were performed on MPCDFs Hydra and Helios at IFERC-CSC.

[1] J. Nührenberg and R. Zille, Phys. Lett. A **129**, 113 (1988).

[2] A.H. Boozer, Plasma Phys. Control. Fusion **37**, A103 (1995).

[3] F.S.B. Anderson, A.F. Almagri, D.T. Anderson, P.G. Mathews, J.N. Talmadge and J.L. Shohet,Fusion Technol. **27**, 273 (1995).

[4] P. Helander and J. Nührenberg, Plasma Phys. Control. Fusion **51**, 055004 (2009).

[5] J. Nührenberg, Plasma Phys. Control. Fusion **52**, 124003 (2010).

[6] C.D. Beidler, G. Grieger, F. Hernegger, E. Harmeyer, J. Kisslinger, W. Lotz, H. Maaßberg, P. Merkel, J. Nührenberg, F. Rau, J. Sapper, F. Sardei, R. Scardovelli, A. Schlüter and H. Wobig, Fusion Technology

17, 148 (1990).

[7] T. Klinger, C. Baylard, C.D. Beidler, J. Boscary, H.S. Bosch, A. Dinklage, D. Hartmann, P. Helander, H. Maßberg, A. Peacock, T.S. Pedersen, T. Rummel, F. Schauer, L. Wegener and R. Wolf, Fusion Eng. Des. **88**, 461 (2013).

[8] J.M. Canik, D.T. Anderson, F.S.B. Anderson, K.M. Likin, J.N. Talmadge and K. Zhai, Phys. Rev. Lett. **98**, 085002 (2007).

[9] C.D. Beidler, K. Allmeier, M.Yu. Isaev, S.V. Kasilov, W. Kernbichler, G.O. Leitold, H. Maaßberg, D.R. Mikkelsen, S. Murakami, M. Schmidt, S.A. Spong, V. Tribaldos and A. Wakasa, Nucl. Fusion **51**, 076001 (2011).

[10] T. Görler, X. Lapillonne, S. Brunner, T. Dannert, F. Jenko, F. Merz, and D. Told, J. Comput. Phys. **230**, 7053 (2011).

[11] T. Görler, A.E. White, D. Told, F. Jenko, C. Holland and T.L. Rhosed, Phys. Plasmas **21**, 122307 (2014).

[12] N.T Howard, A.E. White, M. Greenwald, C. Holland, and J. Candy, Phys. Plasmas **21**, 032308 (2014).

[13] J. Citrin, S. Breton, F. Felici, F. Imbeaux, T. Aniel, J.F. Artaud, B. Baiocchi, C. Bourdelle, Y. Camenen and J. Garcia, Nucl. Fusion **55**, 092001 (2015).

[14] G.G. Plunk, P. Helander, P. Xanthopoulos and J.W. Connor, Phys. Plasmas **21**, 032112 (2014).

[15] P. Xanthopoulos and F. Jenko, Phys. Plasmas **14**, 042501 (2007).

[16] P. Xanthopoulos, F. Merz, T. Görler and F. Jenko, Phys. Rev. Lett. **99**, 035002 (2007).

[17] T.-H. Watanabe, H. Sugama and S. Ferrando-Margalet, Phys. Rev. Lett. **100**, 195002 (2008).

[18] M. Nunami, T.-H. Watanabe and H. Sugama, Phys. Plasmas **20**, 092307 (2013).

[19] G.?G. Plunk, P. Xanthopoulos, and P. Helander, Phys. Rev. Lett. **118**, 105002 (2017).

[20] P. Xanthopoulos, G.?G. Plunk, A. Zocco, and P. Helander, Phys. Rev. X **6**, 021033 (2016)

[21] H.E. Mynick, N. Pomphrey, and P. Xanthopoulos, Phys. Rev. Lett. **105**, 095004 (2010).

[22] H.E. Mynick, N. Pomphrey, and P. Xanthopoulos, Phys. Plasmas **18**, 056101 (2011).

[23] H.E. Mynick, P. Xanthopoulos, B.J. Faber, M. Lucia, M. Rorvig and J.N. Talmadge, Plasma Phys. Control. Fusion **56**, 094001 (2014).

[24] P. Xanthopoulos, H.E. Mynick, P. Helander, Y. Turkin, G.G. Plunk, F. Jenko, T. Görler, D. Told, T. Bird, and J.H.E. Proll, Phys. Rev. Lett. **113**, 155001 (2014).

[25] J.H.E. Proll, P. Helander, G.G. Plunk and J.W. Connor, Phys. Rev. Lett. **108**, 245002 (2012).

[26] P. Helander, J.H.E. Proll, and G.G. Plunk, Phys. Plasmas **20** 122505 (2013).

[27] J.H.E. Proll, P. Xanthopoulos and P. Helander, Phys. Plasmas **20** 122506 (2013).

[28] P. Helander, submitted to J. Plasma Phys (2017).

[29] P. Helander, T. Bird, F. Jenko, R. Kleiber, G.G. Plunk, J.H.E. Proll, J. Riemann and P. Xanthopoulos, Nucl. Fusion **55**, 053030 (2015).

[30] J. L. Luxon, Nucl. Fusion **42**, 614 (2002).

[31] F. Jenko, W. Dorland, M. Kotschenreuther and B.N. Rogers, Phys. Plasmas **7**, 1904 (2000).

[32] P. Xanthopoulos, W. A. Cooper, F. Jenko, Yu. Turkin, A. Runov and J. Geiger, Phys. Plasmas **16**, 082303, (2009).

[33] J.H.E. Proll, H. Mynick, P. Xanthopoulos, S.A. Lazerson and B.J. Faber, Plasma Phys. Control. Fusion **58**, 014006 (2015).

[34] B.J. Faber, M.J. Pueschel, J.H.E. Proll, P. Xanthopoulos, P.W. Terry, C.C. Hegna, G.M. Weir, K.M. Likin and J.N. Talmadge, Phys. Plasmas **22**, 072305 (2015).

[35] H. Smith, private communication

[36] G.G. Plunk, J.W. Connor and P. Helander, submitted to J. Plasma Phys. (2017)